



Removal of Methylene Blue from an Aqueous Medium Using Atemoya Peel as a Low-cost Adsorbent

Adneia de Fátima Abreu Venceslau · Andressa Campos Mendonça ·
Lucas Bragança Carvalho · Guilherme Max Dias Ferreira ·
Sergio Scherrer Thomasi · Luciana Matos Alves Pinto

Received: 12 July 2021 / Accepted: 21 October 2021 / Published online: 31 October 2021
© The Author(s), under exclusive licence to Springer Nature Switzerland AG 2021

Abstract This study prepared a biosorbent from the agricultural waste of atemoya peels, which was then used to remove the methylene blue dye. The atemoya peels were used *in natura*, and some were subjected to an alkaline treatment. The pH values obtained for the points of zero charge were 6.0 and 8.0 for the untreated and alkaline-treated materials, respectively. For neutral and/or alkaline pH values, the untreated and treated materials achieved average removals of approximately 80% and 90%, respectively. A kinetic

study of the model dye removal profile showed a higher removal ratio over a shorter period for the alkaline-treated material. This profile is described by the pseudo-second-order model, which was the best fit for the D-R isotherm in both biosorbents. The maximum biosorption capacities were 190.18 mg g⁻¹ (untreated) and 264.50 mg g⁻¹ (treated) at 45 °C, and the alkaline-treated materials were shown to be reusable for at least 5 cycles. The results show that these biosorbents are efficient and cost-effective to remove the studied model molecules.

Supplementary Information The online version contains supplementary material available at <https://doi.org/10.1007/s11270-021-05414-7>.

Keywords Adsorption · Annona · Biomass · Eco-friendly · Residue · Wastewater treatment

A. d. A. Venceslau · A. C. Mendonça · G. M. D. Ferreira ·
S. S. Thomasi · L. M. A. Pinto (✉)
Department of Chemistry, Federal University of Lavras
(UFLA), 37.200-900, P.O. Box 3037, Lavras, MG, Brazil
e-mail: luca@ufla.br

A. d. A. Venceslau
e-mail: adneiafabreu@yahoo.com.br

A. C. Mendonça
e-mail: andressa-saa@hotmail.com

G. M. D. Ferreira
e-mail: guilherme.ferreira@ufla.br

S. S. Thomasi
e-mail: sergio.thomasi@ufla.br

L. B. Carvalho
Institute of Science and Technology, São Paulo State
University (UNESP), Sorocaba, Brazil
e-mail: lucasuflla@hotmail.com

1 Introduction

Water contamination by different pollutants causes a series of negative impacts on aquatic ecosystems and poses risks to human health, whether due to water or fish consumption from these sources (Dutta et al., 2020; Richardson & Ternes, 2018; Sellaoui et al., 2021a; Sellaoui et al., 2021a, b). This contamination results from high volumes of industrial waste with diverse chemical compositions that is discharged daily into water bodies worldwide (Ferrari et al., 2019; Mateo-Sagasta et al., 2017; Silva et al., 2021). Many studies of contaminants derived from the textile industry and other sectors involving the use of dyes have indicated the potential toxicological risks

of these compounds and their degradation products (Carneiro et al., 2010; Tkaczyk et al., 2020). There are reports of carcinogenic and mutagenic effects that may be cumulative in certain organisms and are capable of causing endocrine disorders (Bafana et al., 2011). However, the major problem related to the disposal of dye-containing waste concerns the dyes themselves. The presence of these compounds in water prevents the penetration of solar radiation and can interfere with the photosynthetic activity of algae and submerged plants, reducing the amount of oxygen available to other aquatic organisms (Tkaczyk et al., 2020).

In this context, adsorption has emerged as a promising method to efficiently remove dyes from wastewater (Smoczyński et al., 2020). However, despite an intense search for new adsorbent materials (Kumara et al., 2019), finding a material that is easily obtained, abundant, has a good adsorption capacity, and is low cost is still a challenge. Therefore, natural compounds such as agricultural waste, which is usually improperly discarded, have emerged as promising candidates for the development of new adsorbents, known as biosorbents (Fomina & Gadd, 2014). Numerous types of biomass can be used as biosorbents, including rice husks (Vithanage et al., 2016), malt bagasse (Juchen et al., 2018), sisal fibers (Khadir et al., 2020), wolf apples (Araújo et al., 2018), dairy cattle manure (Tsai et al., 2019), marine algae (El-Naggar & Rabei, 2020; Mokhtar et al., 2017), invasive macrophytes (Pérez-Morales et al., 2019), geopolymer monoliths (Novais et al., 2018), and Roger mushrooms (Kariuki et al., 2017), among others.

Atemoya is a hybrid fruit produced from an artificial cross-breeding between the sweetsop (*Annona squamosa* L.) found in dry climates and a species of cherimoya (*Annona cherimola* Mill.), which grows in high-altitude tropical climates (Morton, 1987). The fruits of the atemoya weigh ~300 g and have a pleasant taste and aroma, with sensory characteristics superior to those of the sweetsop and cherimoya (Baron et al., 2018). They are usually consumed *in natura*, but because of their considerable perishability, some forms of processing have been considered, such as juices, jellies, jams, and purées, and storage as frozen or freeze-dried products (de Souza et al., 2015). During processing, which values the pulp of the atemoya fruit, large amounts of byproducts are generated and discarded (Silva et al., 2016). These

residues include the rough green peel, which accounts for between 28 and 50% of the mass of the fruit (Cruz et al., 2013). This waste is a low-cost raw material with the potential for several applications that could add value to the atemoya crop.

Methylene blue is a low toxicity cationic dye that is difficult to degrade (Cooksey, 2017). This dye is widely used in the laboratory to identify the adsorption capacity of most distinct adsorbents (Biehl et al., 2018). Owing to its strong absorption in the UV–visible light region of the spectrum, high solubility, and properties similar to textile dyes, it has been widely used as a model compound for organic contaminants and in oxidation reactions (Rafatullah et al., 2010). Based on the above considerations, the objective of this study was to prepare a new biosorbent from agricultural waste consisting of atemoya peels. The removal efficiency of the obtained material was evaluated using an adsorption study of the methylene blue model molecule in aqueous solutions.

2 Materials and Methods

2.1 Preparation of the Biosorbent

Fresh atemoya fruits of the Thompson variety (Exsiccata ESAL 30.249) were purchased from a local rural producer (Lavras/MG) during the 2016–2017 harvest (Venceslau et al., 2021). The biosorbents were prepared from the peels, following the methodology of Carvalho et al. (2018). After removing the pulp, the atemoya peels were oven-dried at 70 °C and crushed in a knife mill with a 150 mesh particle size. After this process, a portion of the material was stored in hermetically sealed flasks (“untreated”). The remaining material was mixed with a 1 mol L⁻¹ NaOH solution, stirred for 12 h and vacuum filtered, washed with distilled water to a neutral pH, and dried in an oven at 60 °C for 48 h. This material was then stored in hermetically sealed flasks for further characterization (“treated”).

2.2 Biosorbent Characterization

The biosorbent materials were characterized using UV spectroscopy, thermogravimetric analyses, and

morphological analyses with scanning electron microscopy.

A Digilab Excalibur Fourier transform infrared spectrometer (FTS 3000 series) was used to obtain the absorption spectra in the infrared region using KBr optical windows. In addition to the prepared biosorbents, 10 mg samples of the materials were analyzed after they were exposed to methylene blue (50 mg L⁻¹, pH 7.00) under constant stirring for 12 h at 150 rpm at room temperature (25 ± 2 °C), then filtered and dried in an oven at 40 ± 2 °C for 24 h. The spectra were obtained in the range of 4000–400 cm⁻¹, with 8 cm⁻¹ resolution and an accumulation number of 32 scans.

Thermogravimetric analyses of the biosorbents were performed in an N₂ atmosphere using a Shimadzu Model 60 AH system with temperatures ranging between 25 and 700 °C, a gas flow of 30 mL min⁻¹, an initial sample mass of ~5 mg, and a 10 °C min⁻¹ heating rate.

Morphological analyses were performed using a LEO EVO 40XVP scanning electron microscope. The samples of the prepared biosorbents were arranged in aluminum stubs and covered with colloidal gold in an argon atmosphere in a vacuum for 180 s in a Balzers Sputter Coater SCD 050. After this procedure, the electron micrographs were obtained.

2.3 Adsorption and Desorption Studies

Studies of the effect of solution pH on the adsorption process used 20 mg of each biosorbent dispersed in 10 mL of a 20 mg L⁻¹ dye solution. The pH of the initial reaction medium was adjusted using 0.025 mol L⁻¹ HCl and 0.1 mol L⁻¹ NaOH solutions. Analyses at pH values of 1.00, 2.00, 3.00, 4.00, 5.00, 6.00, 7.00, 8.00, 9.00, 10.00, 11.00, and 12.00 were conducted. The systems were agitated at room temperature (25 ± 2 °C) for 12 h at 150 rpm and centrifuged for 5 min at 3500 × g, after which the supernatant was collected for analysis. The amount of adsorbed dye was calculated using Eq. 1:

$$q_e = \frac{(C_i - C_e)V}{m} \quad (1)$$

where q_e (mg g⁻¹) is the amount of adsorbed methylene blue, V (L) is the solution volume, C_i and C_e (mg L⁻¹) are the initial and final dye concentrations,

respectively, and m (g) is the mass of the adsorbent. The percentage removed was calculated using Eq. 2:

$$\% \text{biosorption} = \frac{C_i - C_e}{C_i} \times 100 \quad (2)$$

To determine the pH_{ZCP}, 10 mg of each adsorbent was added to 10 mL of a 0.100 mol L⁻¹ aqueous KCl solution, under 12 different initial pH conditions (1.00, 2.00, 3.00, 4.00, 5.00, 6.00, 7.00, 8.00, 9.00, 10.00, 11.00, and 12.00). The pH was adjusted using 0.1 mol L⁻¹ HCl or NaOH solutions. After agitation in a thermostatic bath at 25 ± 2 °C for 24 h, the samples were filtered and the final pH of the solution was measured. The ΔpH_{ZCP} was obtained from the difference between the initial and final pH values.

A 20 mg sample of each biosorbent was transferred to 50-mL flasks for the adsorption kinetics analyses. Then, 20 mL of the 50 mg L⁻¹ dye solution was added. At predetermined intervals (0, 2, 5, 10, 15, 20, 25, 30, 40, 50, 60, 90, 120, 150, 180, and 210 min), 200 μL aliquots of the solution were collected and diluted in 5000 μL of deionized water, after which the dye concentration was measured. The experiments were conducted under continuous stirring at 150 rpm at four different temperatures (25, 35, 45, and 55 °C) and at a pH of 7.00.

Adsorption equilibrium analyses were conducted by dispersing 10 mg of each atemoya biosorbent into 10 mL of dye solutions with different initial concentrations (10, 25, 50, 75, 100, 150, and 200 mg L⁻¹) at a pH of 7.00. The samples remained under continuous stirring (150 rpm) for 12 h at 25, 35, 45, and 55 °C. Afterwards, they were centrifuged for 5 min at 3500 × g and the supernatant was collected to determine the equilibrium concentration of the dye.

For desorption analyses, samples of each biosorbent were loaded with methylene blue as in the adsorption experiments (10 mg biosorbent, 10 mL of a 50 mg L⁻¹ methylene blue solution, stirred at 150 rpm for 1 h, at pH 7.00 and 25 ± 2 °C). The mixture of the biosorbent and the loaded dye was centrifuged for 5 min at 3500 × g, the supernatant was removed, and the amount of adsorbed dye was determined using Eq. 1. Then, 10 mL of 0.200 mol L⁻¹ HCl solution was added to the dye-loaded material and agitated for 1 h at 150 rpm. Finally, a 200 μL aliquot of the supernatant was removed and diluted in 5000 μL of deionized water to determine the desorbed dye

concentration. The remaining material was vacuum filtered and washed with deionized water up to pH 7.00. and reused in batches for 5 successive adsorption/desorption cycles.

All adsorption tests were performed in triplicate and the quantification of the methylene blue in the solutions was performed using UV–vis molecular absorption spectrophotometry at a 665 nm wavelength.

3 Results and Discussion

3.1 Biosorbent Characterization

3.1.1 Infrared Spectroscopy

The surface of a chemically modified biosorbent can modulate the specific number of active bonding sites in the material, improving its ion exchange properties and its adsorption capacity (Ramrakhiani et al., 2016). Infrared spectroscopy can provide important information on the chemical modifications due to the alkaline treatment of the biosorbents obtained from the atemoya peels. Figure 1 shows the infrared spectra of the prepared biosorbents. The main functional groups on the surfaces of these materials that influence adsorption behavior can be identified.

The wide bands between 3000 and 3600 cm^{-1} observed in the infrared spectra of the alkaline-treated and untreated atemoya peel materials are related to the vibrational elongation of the O–H bond of the hydroxyls in lignin, cellulose, and water (Mohamed et al., 2017; Tran et al., 2017). The band at 2920 cm^{-1} in both spectra corresponds to the strain vibrations of C–H bonds in alkanes, aliphatic acids, and aldehydes, which are bonds of cellulose, hemicellulose, and lignin structures (Gerola et al., 2013; Sadaf & Bhatti, 2014). The band at 1724 cm^{-1} is related to the symmetrical stretching of the keto tautomer of carbonyl C=O in cellulose, hemicellulose, and lignin (Schwanninger et al., 2011) and is present only in the spectrum of the untreated biosorbent. This band disappears after alkaline treatment, suggesting that this process partially removes the non-cellulosic compounds from the atemoya peel. Accordingly, the band related to the elongation vibration of the C=C bonds in the aromatic rings of the lignin structure, observed at 1605 cm^{-1} in the untreated material,

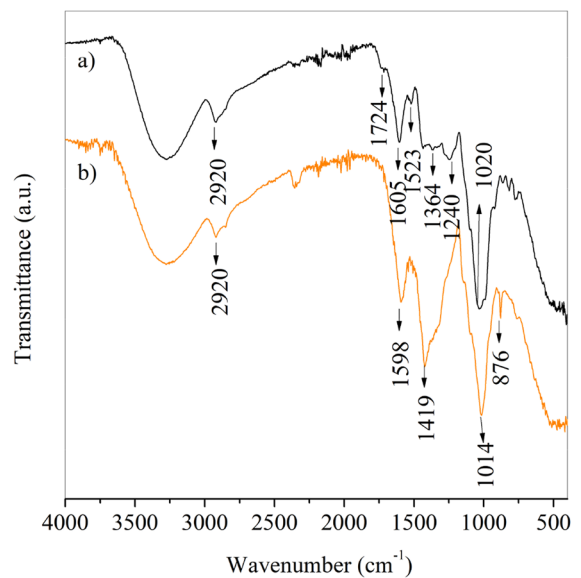


Fig. 1 Infrared spectra of the atemoya biosorbent samples that were (a) untreated and (b) alkaline-treated

shifted to 1598 cm^{-1} after alkaline treatment. This confirms that a compositional modification is caused by the alkaline treatment applied to the atemoya peel and is related to the partial solubilization of lignin (Costa et al., 2006).

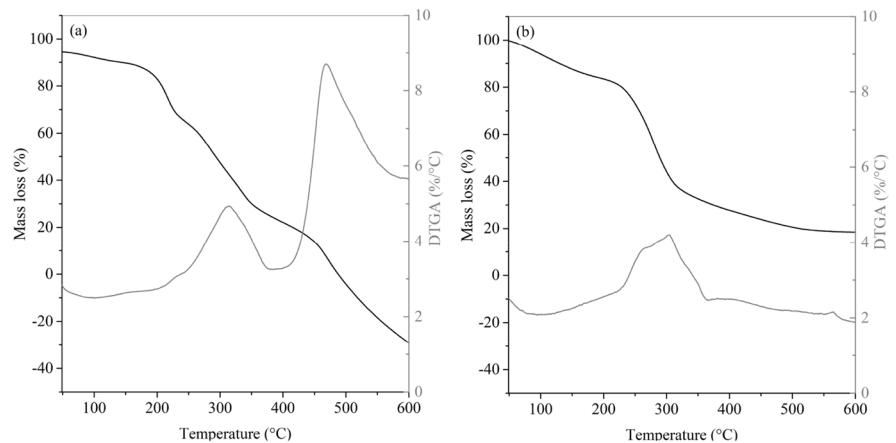
This hypothesis is also corroborated by observed changes in the biosorbent spectra at 876 and 1014 cm^{-1} . The band at 1014 cm^{-1} is associated with cellulose and hemicellulose C–O vibrations (Mohtar et al., 2015), as well as aromatic and vinyl ethers present in the flavonoids characteristic of the *Annona* species, and appeared after the alkaline treatment. In the material *in natura*, this band is superimposed on the 1020 cm^{-1} band and is associated with the angular deformation vibrations of C–H bonds in the planes of lignin aromatic rings. In addition, the bands at 1423 and 1364 cm^{-1} in both spectra, with differing intensities, correspond to the angular deformations of –CH₃ and –CH₂ adjacent to carbonyl, respectively.

3.1.2 Thermogravimetric Analyses

Thermogravimetric analyses (TGA) were performed to assess the thermal stability of the untreated (Fig. 2-a) and alkaline-treated (Fig. 2-b) biosorbents.

The TGA thermogram profiles of the materials were very different, confirming that the alkaline

Fig. 2 Thermogravimetric analyses of the (a) untreated and (b) alkaline-treated atemoya biosorbent



treatment modified the composition of the biosorbent. The elimination of low molar mass volatile compounds and surface-adsorbed water from the biosorbent occurred between 50 and 183 °C in the untreated material (Fig. 2-a) and between 50 and 229 °C in the alkaline-treated material (Fig. 2-b), with 14 and 20% losses in mass, respectively.

The thermal decomposition stages of the materials were observed at temperatures above those at which volatilization compounds were eliminated. For biomass *in natura*, the stages at which the largest mass losses occurred started at 270 °C and were associated with the decomposition of the extractives composed of hemicellulose (271 °C, 58%) and cellulose (315 °C, 42%). The decomposition of lignin and other compounds occurred above 466 °C (8%) (Shanmugarajah et al., 2019), and at 488 °C the material was completely degraded.

The thermal stability of the material increased after the alkaline treatment, starting at 314 °C (38%). This was probably due to the loss of part of the hemicellulose content, which has a lower thermal stability than cellulose (Singh et al., 2015) possibly due to a lower crystallinity. The complete decomposition of the organic material in the alkaline-treated biosorbent occurred at 600 °C. Above this temperature (data not shown), the mass remained constant, leaving ~20% of the mass as ash. The production of ash in the decomposition process indicates that the protonated acid groups of the material *in natura* were ionized during the alkaline treatment, leading to the formation of complexes with sodium ions.

3.1.3 Scanning Electron Microscopy

The microstructures of the untreated (Fig. 3-a) and alkaline-treated atemoya biosorbents (Fig. 3-b) were observed using scanning electron microscopy at 300× magnification.

The material *in natura* (Fig. 3-a) exhibited an irregular surface, with cracks and pores of varying diameters and depths, many of which were obstructed, characterizing a heterogeneous surface. After the alkaline treatment, the material exhibited a rougher surface (Fig. 3-b). Moreover, the treatment seems to have promoted the opening of the pores, leading to a larger specific surface area that was configured as a favorable modification for the adsorption of larger molecules in solution. This process must have been associated with the dissolution of lignocellulosic and hemicellulose components by the NaOH solution, which can cause swelling of the fibers and results in an increase in the internal surface area (Rojo et al., 2013). These observations suggest that treating atemoya peels with 1 mol L⁻¹ NaOH modified the biomass properties that favor their use in adsorption processes, as previously reported in studies of other adsorbents (Chieng et al., 2017).

3.2 Effect of pH on Methylene Blue Removal Capacity

pH is an important parameter regarding the removal capacity of an adsorbent, as it affects both the adsorbate charge distribution in the solution and the adsorbent surface charge distribution, especially

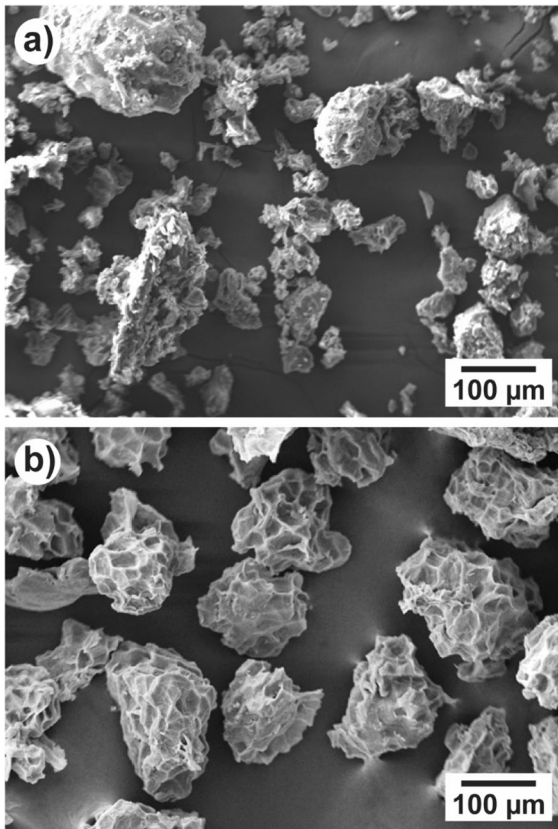


Fig. 3 Scanning electron microscope images of the (a) untreated and (b) alkaline-treated atemoya peels

because of the protonation/deprotonation processes of the acid and basic surface functional groups (Carvalho et al., 2019). Thus, the pH of the zero-charge point (pH_{ZCP}) is an important parameter for obtaining qualitative information about the liquid charge of an adsorbent as a function of pH, enabling the understanding of adsorption behavior at different pH values. The pH_{ZCP} of the untreated (*in natura*) and alkaline-treated materials were determined using the solid addition method, as shown in Fig. 4.

The untreated and alkaline-treated materials had pH_{ZCP} values of 5.15 and 7.48, respectively. At pH values below the pH_{ZCP} , the adsorbent surface has a positive liquid charge, with a greater capacity for adsorbing anionic species, while above the pH_{ZCP} , the liquid charge is negative, favoring the adsorption of cationic species such as methylene blue (Regalbuto & Robles, 2004).

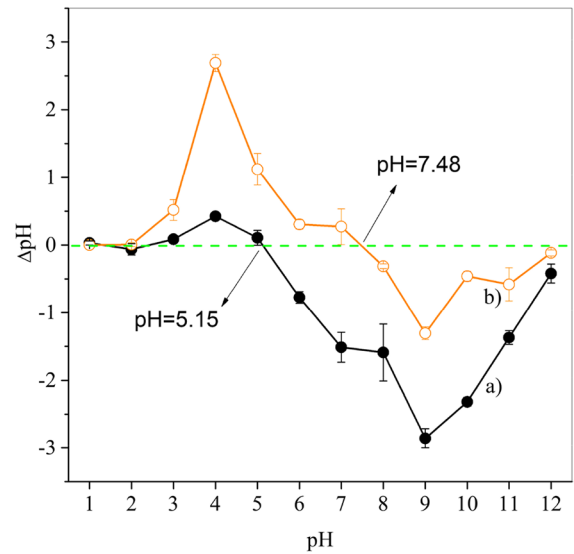


Fig. 4 pH of zero-charge points (pH_{ZCP}) of the (a) untreated and (b) alkaline-treated atemoya biosorbents.

The increase in the pH_{ZCP} of the modified material is in accordance with the loss of organic matter content (hemicelluloses and lignin), which resulted in the loss of acid groups with low pK_a values in hemicelluloses and a consequent increase in the specific number of basic sites of the material. Although the working pH range suitable for cation adsorption decreased in the modified biosorbent (i.e., a $\text{pH} > 7.48$ compared to a $\text{pH} > 5.15$ of the untreated material), it is expected that neutral to slightly basic media will result in a good removal capacity for the alkaline-treated material. The reason for this is that the microstructural modification of the biosorbent promoted by the alkaline treatment can compensate for the loss of the acid groups. Analyses of the effect of pH on the adsorption of methylene blue by the biosorbents were conducted to confirm this hypothesis and are presented in Fig. 5.

For both adsorbents, the percentage of biosorption increased with an increase in pH, remaining constant for pH values above 5.00. The material *in natura* yielded dye removal capacities of 81–88% in a pH range of 5.00–12.00, while the alkaline-treated material yielded removal capacities of 86–94% in the same pH range. Although the removal of methylene blue using the modified biosorbent at higher pH values was more efficient, the material *in natura* adsorbed the methylene blue better at pH values below 3.00.

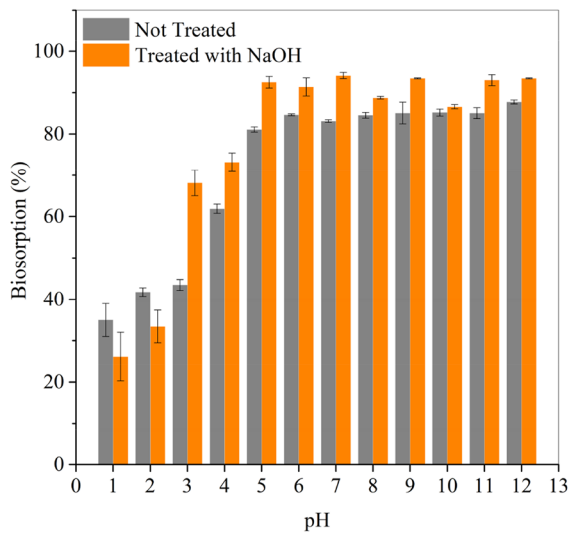


Fig. 5 Effect of pH on the removal of methylene blue (20 mg L^{-1}) by biosorbents obtained from atemoya peels. The mixtures were stirred at room temperature ($25 \pm 2 \text{ }^\circ\text{C}$) for 12 h at 150 rpm

This suggests that a change in the surface charge density of the materials occurred that was mediated by the pH.

According to Yanishpolskii et al. (2000), the pK_a value of the methylene blue molecule cannot be experimentally determined since it is above a pH of 13.00. Its high alkalinity forces its ions to behave in a similar manner as alkaline metal ions, holding a positive charge in all investigated pH ranges. Thus, the lower removal percentages of the methylene blue model dye for pH values below 5.00 result from electrostatic repulsion between the adsorbate and the surface of the adsorbents (also positively charged), since in this range the pH is lower than the pH_{ZCP} values of the two biosorbents.

At pH values of 1.00 and 2.00, the removal of part of the hemicellulose and lignin fractions from the treated material increased the specific fraction of protonable sites on its surface. This promoted a greater competition of H^+ ions at high concentrations at the adsorption sites on the material, increasing the positive surface charge and leading to lower removal percentages than those of the untreated material. When the pH was increased to 3.00, the positive surface charge was reduced, decreasing the electrostatic repulsion between the dye and the surface while reducing the competition of H^+ ions at the adsorption

sites. Under these conditions, the alkaline-treated material had the highest methylene blue dye removal rates, reinforcing the concept that the alkaline treatment modified the microstructure of the material.

A pH of 7.00 was chosen for the other analyses because it yielded high removal percentages and does not require a pH adjustment for disposal after biosorbent use in potential textile effluent dye removal applications.

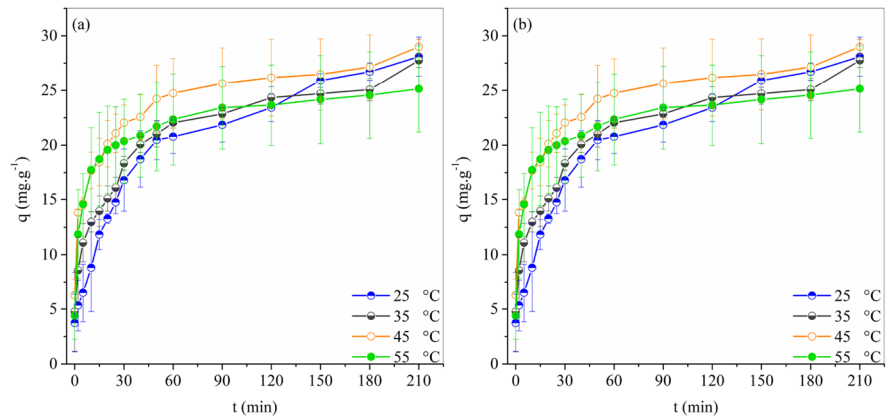
3.3 Adsorption Kinetics

Evaluating the kinetic parameters is an important factor for describing the effectiveness of an adsorption process. The kinetic model cannot only estimate the adsorption rate, but can also provide evidence of the possible mechanisms involved (Foo & Hameed, 2009; Kwak et al., 2019). The kinetic adsorption behaviors of the methylene blue model molecule in untreated (Fig. 6-a) and alkaline-treated biosorbents (Fig. 6-b) were monitored for 210 min at a pH of 7.00 and at temperatures of 25, 35, 45, and 55 $^\circ\text{C}$.

The results of the methylene blue adsorption kinetics analyses for both biosorbents indicated a rapid adsorption process in which the highest adsorption rates occurred in the first 60 min of contact between the adsorbent and the adsorbate. Equilibrium was reached at 150 min for both untreated and alkaline-treated materials at 25 $^\circ\text{C}$. This decreased to 90 min for the untreated material and 120 min for the alkaline-treated material when the temperature reached 55 $^\circ\text{C}$. Franco et al. (2020) also identified this biosorption profile when working with *Annona crassiflora* seeds, which has a kinetic profile that shows initial rapid dye removal from the solution, followed by a slower removal process. This can be explained by the fact that more adsorption sites are available on the biosorbent surface (Kilic et al., 2011).

Several kinetic models were used to determine the adsorption mechanism. This study evaluated the pseudo-first-order (Lagergren, 1898; Rudzinski & Plazinski, 2007), pseudo-second-order (Ho & McKay, 1999; Rudzinski & Plazinski, 2007), and intraparticle diffusion (Weber & Morris, 1963) models. The pseudo-first-order model assumes non-dissociated molecular adsorption on the surface of the material (Lagergren, 1898; Rudzinski & Plazinski, 2007) and is expressed linearly using Eq. 3.

Fig. 6 Effect of contact time on methylene blue removal at different temperatures for the (a) untreated and (b) alkaline-treated atemoya biosorbents. The mixtures were stirred for 210 min at 150 rpm, an initial pH of 7.00, and an initial 50 mg L⁻¹ dye concentration



$$\frac{q_t}{q_e} = e^{-k_1 t} \tag{3}$$

where q_t (mg g⁻¹) is the adsorption amount at time t (min), q_e (mg g⁻¹) is the amount adsorbed at equilibrium, and k_1 (min⁻¹) is the pseudo-first-order speed constant. The kinetic parameters for this model were obtained by plotting $\ln(q_e - q_t)$ vs. t .

The pseudo-second-order model assumes an adsorption process by chemisorption (Ho & McKay, 1999; Rudzinski & Plazinski, 2007) and is expressed in its non-linear form as:

$$q_t = \frac{q_e^2 k_2 t}{1 + k_2 t q_e} \tag{4}$$

where q_t (mg g⁻¹) is the adsorption amount at time t (min), q_e (mg g⁻¹) is the amount adsorbed at equilibrium, and k_2 (min⁻¹) is the pseudo-second-order constant rate. The kinetic parameters were obtained by plotting $1/q_t$ vs. t .

The intraparticle diffusion model assumes that adsorption depends on the transfer rate of the adsorbate from the solution phase to the surface of the adsorbent particles, and is controlled by one or more steps (e.g., film or external diffusion, pore diffusion, and surface diffusion) (Weber & Morris, 1963). The model is expressed by:

$$q_t = k_{int} t^{1/2} + C \tag{5}$$

where k_{int} is the intraparticle diffusion speed constant (mg g⁻¹ min^{-1/2}) and C (mg g⁻¹) is the intersection of the straight line with the ordinate axis. The value of C provides a quantitative relationship with the thickness of the diffusion limit layer (i.e., the higher the

value of C , the greater the effect of the limit layer). By plotting q_t versus $t^{1/2}$, it is possible to calculate the slope of the line, k_{int} . A plot of the intraparticle diffusion model generally exhibits multi-linearity, indicating that two or more adsorption steps can occur. The first step represents immediate adsorption, the second step is a gradual phase, and the third is the final equilibrium phase where speed reduction occurs (Lin & Juang, 2002).

The validity of each model was evaluated using the obtained linear regression data, including the correlation coefficient (R^2) and the root mean square (RMS) function, defined by:

$$RMS = \frac{\sqrt{\sum_{i=1}^n (y^{\wedge} - y)^2}}{n} \tag{6}$$

where y^{\wedge} are the experimentally determined values, y are the values predicted by the model, and n is the number of analyzed data points. Table 1 shows the evaluated kinetic model parameters and Figs. S1, S2, S3, and S4 (Supplementary material) present the graphs with the appropriate adjustments.

Based on the correlation coefficient ($R^2 > 0.9662$) and RMS (RMS < 0.046) values, the kinetic studies indicate that the pseudo-second-order model provided the best adjustments for the experimental data of both treated and untreated materials independent of the adsorption temperature. This indicates that the reaction mechanism was kinetically controlled by chemical adsorption. The occurrence of chemisorption suggests an exchange or sharing of electrons between the functional groups on the surface of the biosorbent and the methylene blue (Rangabhashiyam et al., 2018). The second-order speed constants increased

Table 1 Kinetic adsorption parameters of the biosorbents for the methylene blue model molecule

Untreated biosorbent					
Pseudo-first order					
<i>T</i> (K)	$q_{e\ exp}$ (mg g ⁻¹)	$q_{e\ calc}$ (mg g ⁻¹)	k_1 (min ⁻¹)	R^2	<i>RMS</i>
298.15	29.33	21.45	1.26×10^{-02}	0.9678	0.130
308.15	28.02	18.09	1.49×10^{-02}	0.8570	0.143
318.15	32.02	15.13	7.66×10^{-03}	0.8499	0.187
328.15	27.22	10.85	8.79×10^{-03}	0.8208	0.194
Pseudo-second order					
<i>T</i> (K)	$q_{e\ exp}$ (mg g ⁻¹)	$q_{e\ calc}$ (mg g ⁻¹)	k_2 (g mg ⁻¹ min ⁻¹)	R^2	<i>RMS</i>
298.15	29.33	30.86	1.29×10^{-03}	0.9911	0.018
308.15	28.02	28.60	2.23×10^{-03}	0.9928	0.029
318.15	32.02	30.51	2.90×10^{-03}	0.9890	0.030
328.15	27.22	26.41	4.65×10^{-03}	0.9953	0.026
Intraparticle diffusion line 1					
<i>T</i> (K)	C_2 (mg g ⁻¹)		k_{int} (mg g ⁻¹ min ^{-1/2})	R^2	
298.15	1.99		2.57	0.9728	
308.15	5.45		2.22	0.9895	
318.15	9.40		2.19	0.9276	
328.15	7.08		3.36	0.9999	
Intraparticle diffusion line 2					
<i>T</i> (K)	C_2 (mg g ⁻¹)		k_{int} (mg g ⁻¹ min ^{-1/2})	R^2	
298.15	11.47		1.14×10^0	0.9719	
308.15	14.49		8.65×10^{-1}	0.8844	
318.15	15.70		9.50×10^{-1}	0.7887	
328.15	17.23		5.90×10^{-1}	0.9550	
Treated biosorbent					
Pseudo-first order					
<i>T</i> (K)	$q_{e\ exp}$ (mg g ⁻¹)	$q_{e\ calc}$ (mg g ⁻¹)	k_1 (min ⁻¹)	R^2	<i>RMS</i>
298.15	37.50	25.75	7.62×10^{-3}	0.9064	0.155
308.15	36.96	28.05	8.74×10^{-3}	0.9823	0.137
318.15	39.75	32.75	1.10×10^{-2}	0.9871	0.113
328.15	43.31	38.40	1.48×10^{-2}	0.9917	0.084
Pseudo-second order					
<i>T</i> (K)	$q_{e\ exp}$ (mg g ⁻¹)	$q_{e\ calc}$ (mg g ⁻¹)	k_2 (g mg ⁻¹ min ⁻¹)	R^2	<i>RMS</i>
298.15	37.50	36.53	1.03×10^{-3}	0.9759	0.046
308.15	36.96	37.40	8.11×10^{-3}	0.9662	0.041
318.15	39.75	42.61	6.27×10^{-4}	0.9760	0.038
328.15	43.31	49.11	5.20×10^{-4}	0.9861	0.026
Intraparticle diffusion line 1					
<i>T</i> (K)	C^1 (mg g ⁻¹)		k_{int} (mg g ⁻¹ min ^{-1/2})	R^2	
298.15	2.11		3.06	0.9038	
308.15	4.54		2.20	0.9907	
318.15	1.97		2.94	0.9752	
328.15	0.62		3.41	0.9843	
Intraparticle diffusion line 2					
<i>T</i> (K)	C^2 (mg g ⁻¹)		k_{int} (mg g ⁻¹ min ^{-1/2})	R^2	
298.15	8.14		1.74	0.8362	
308.15	3.02		2.12	0.9669	
318.15	5.64		2.20	0.9911	
328.15	13.45		1.99	0.9289	

with increasing system temperatures, indicating that an activation energy needs to be supplied for this specific interaction between the adsorbate and adsorbent sites to occur. Removal of methylene blue using *Agrobacterium fabrum* biomass (Sharma et al., 2018) and using apple peels (Enniya & Jourani, 2017), as well as the removal of copper ions using *Annona squamosa* L. seeds (Sivakumar et al., 2019), exhibits kinetic behaviors similar to those observed in this study.

The intraparticle diffusion graphs (q_t vs. $t^{1/2}$ curves) for the dye adsorption by the adsorbents exhibited two stages (Figs. S5 a, b, c, and d and S6 a, b, c, and d). The lines representing the first stage of adsorption did not cross the origin (C_1 S5 a, b, c, and d and S6 a, b, c, and d). The lines representing the first stage of adsorption did not cross the origin (ON USING biosorbents. The obtained k_{int} values increased with temperature in the case of the treated material; however, the untreated material exhibited the opposite behavior. This suggests that the solvent layer around the surface of the material has distinct water molecule solvation structures, probably due to differences in hydrophobicity promoted by the removal of more hydrophilic compounds during the heat treatment. In the final equilibrium stage (second linear region in the q_t vs. $t^{1/2}$ graph), diffusion through the film decreased because of the low dye concentration in the solution and a low number of available adsorption sites on the surface of the biosorbents.

3.4 Adsorption Isotherms

Adsorption isotherms provide important information for describing how the adsorbate interacts with active sites on the surface of the adsorbents. The adsorption isotherms of the investigated biosorbents for methylene blue dye are presented in Fig. 7.

The isotherms obtained for the untreated and alkaline-treated biosorbents have ascending profiles with a decrease in the adsorption rate with C_e , which can be explained by a decrease in the availability of adsorption sites as the equilibrium concentration increases. In the case of the untreated biosorbent (Fig. 7-a), at lower equilibrium concentrations the temperature did not affect the amount adsorbed. As the equilibrium concentration increased, the temperature increase

slightly increased the amount adsorbed. In the case of the alkaline-treated biosorbent isotherms (Fig. 7-b), the adsorption was constant at all temperatures and an equilibrium concentration of 75 mg L^{-1} .

The experimental methylene blue adsorption data were adjusted using the linear forms of the Langmuir, Freundlich, Dubinin-Radushkevich, and Temkin models. The Langmuir model is valid for monolayer adsorption on a homogeneous surface (Langmuir, 1916) and is represented by Eq. 7.

$$\frac{C_e}{q_e} = \frac{1}{q_m K_L} + \frac{1}{q_m} C_e \quad (7)$$

where q_e is the amount adsorbed at equilibrium (mg g^{-1}), C_e is the dye equilibrium concentration of the solution (mg L^{-1}), K_L is the Langmuir constant, and q_m represents the maximum adsorption capacity (mg g^{-1}).

The Freundlich model adequately describes the adsorption on energetically heterogeneous surfaces with the linear form of the Freundlich isotherm (Freundlich, 1907) as shown in Eq. 8:

$$\ln q_e = \ln K_F + \frac{1}{n_F} \ln C_e \quad (8)$$

where q_e and C_e have the same meaning as those parameters in the Langmuir isotherm and K_F and n_F are the constants related to the Freundlich adsorption capacity and intensity, respectively.

The Dubinin-Radushkevich (D-R) isotherm is similar to the Langmuir isotherm with respect to adsorption occurring in a single layer. However, it is more general because it does not assume a homogeneous surface or a constant adsorption potential (Balarak et al., 2017; Chen & Yang, 1994; Dada et al., 2012). Equation 9 is the linear expression of the D-R isotherm:

$$\ln q_e = \ln q_s - K_{DR} \varepsilon^2 \quad (9)$$

where q_e is the amount of adsorbed solute and q_s is the adsorption capacity, both in mg g^{-1} , and K_{DR} is the constant associated with the adsorption energy ($\text{mol}^2 \text{ kJ}^{-2}$). The parameter ε is the Polanyi potential and is given by $RT \ln [1 + (1/C_e)]$.

Finally, the Temkin model considers the effects of indirect interactions between the adsorbate

molecules on the surface of the adsorbent, assuming that the variation in adsorption enthalpy decreases linearly as the dye adsorbs (Balarak et al., 2017; Dada et al., 2012; Temkin & Pyzhev, 1940). The Temkin isotherm in its linear form is given by Eq. 10:

$$q_e = b_T \ln K_T + b_T \ln C_e \quad (10)$$

where parameters q_e and C_e have the same meanings as in the Langmuir isotherm, K_T is the bonding equilibrium constant ($L \text{ g}^{-1}$) and b_T is a constant associated with the variation in adsorption enthalpy. Table 2 shows the adjusted isotherm parameters for all of the evaluated models in the studied mixtures. Figures S7, S8, S9, S10, S11, S12, S13, and S14 (Supplementary material) display the adjustments made for each model.

In general, the D-R model presented the best adjustments (high R^2 values with lower RMS values) for both biosorbents at temperatures of 308.15 and 318.15 K. At 298.15 K, the Freundlich model provided the best adjustments for both materials, while at 328.15 K, the isotherm obtained for the material *in natura* fit the Langmuir model better, and the isotherm obtained for the modified material fit the Freundlich model better. Nevertheless, at these temperature extremes, the D-R model also yielded good adjustments and could be used to explain the dye adsorption process on the biosorbents at the evaluated conditions, suggesting an adsorption process involving heterogeneous sites. It is interesting to note that the K_{DR} value tends to be lower at the highest temperatures, indicating larger variations in adsorption free energy under this thermodynamic condition.

The q_m parameter in the Langmuir equation allows the estimation of the maximum adsorption capacities of the biosorbents, which were 190.18 mg g^{-1} and 264.50 mg g^{-1} for the untreated and alkaline-treated biosorbents, respectively. A comparison between these capacities and those of other biosorbents studied recently is presented in Table 3, showing that the biosorbents made from the atemoya peel, both alkaline-treated and untreated, can be considered good alternatives for remediating water contaminated with cationic dyes.

3.5 Desorption Analyses

The reuse of adsorbents is of great importance, as it enables economically viable pollutant removal in water treatment processes. The desorption analyses consisted of removing the methylene blue molecules previously adsorbed, allowing the biosorbent to be reused for the next cycle. Figure 8 shows the dye removal profile for five cycles of adsorption and desorption.

The adsorption efficiency for the untreated material was reduced from 61.06 to 41.14% from the first to the second adsorption cycle, remaining practically constant for additional cycles. This may be related to the strong chemical interactions between some functional groups on the untreated material surface and the methylene blue cations. Functional groups are likely capable of developing specific interactions, such as carboxylic groups negatively charged to hemicelluloses. The remaining dye in the untreated material was experimentally visible, since the material had a very dark color (close to black) at the end of the fifth cycle after 1 h of desorption.

The adsorption and desorption efficiencies of the alkaline-treated material remained high for all 5 cycles, presenting only small decreases in removal efficiency from 93.82 to 84.96% and from 92.28 to 82.65% in desorption percentages. In general, the reuse of the modified material proved feasible, since the average efficiencies of the adsorption and desorption processes of the alkaline-treated material were above 80%, indicating the material's potential for low-cost application use.

3.6 Infrared Spectra After Adsorption of Methylene Blue

The infrared spectra for the untreated and alkaline-treated materials filled with the adsorbed dye are shown in Fig. 9.

Figure 9 shows a significant decrease in the $3100\text{--}3400 \text{ cm}^{-1}$ peak for both biosorbents related to OH vibrational stretching, leading to the belief that this functional group participated in the methylene blue adsorption process. Furthermore, band shifts were observed (Table 4), indicating interactions between methylene blue and both the alkaline-treated

Table 2 Adsorption isotherms of the biosorbents for the methylene blue model molecule. Methylene blue concentrations (10; 25; 50; 75; 100; 150; and 200 mg L⁻¹), initial pH=7.00, 12 h stirring at 150 rpm

Untreated					
Langmuir					
T (K)	q_m (mg g ⁻¹)	K_L (L mg ⁻¹)	R^2	RMS	
298.15	177.89	1.69×10^{-2}	0.7244	0.076	
308.15	157.08	4.62×10^{-2}	0.9420	0.070	
318.15	190.18	3.03×10^{-2}	0.9688	0.035	
328.15	168.00	4.59×10^{-2}	0.9501	0.067	
Freundlich					
T (K)	n_F	K_F [mg g ⁻¹ (L mg ⁻¹) ^{1/n}]	R^2	RMS	
298.15	1.48	5.39	0.9873	0.036	
308.15	1.59	9.97	0.9359	0.078	
318.15	1.40	7.48	0.9702	0.057	
328.15	1.51	9.87	0.9235	0.091	
D-R					
T (K)	q_s (mol kg ⁻¹)	K_{DR} (kJ ² mol ⁻²)	R^2	RMS	E (kJ mol ⁻¹)
298.15	2.961	5.37×10^{-3}	0.9776	0.048	1.04×10^{-1}
308.15	3.665	4.62×10^{-3}	0.9503	0.070	9.61×10^{-2}
318.15	5.429	4.97×10^{-3}	0.9825	0.044	9.97×10^{-2}
328.15	4.695	4.31×10^{-3}	0.9440	0.078	9.28×10^{-2}
Temkin					
T (K)	b_T (mol kg ⁻¹)	K_T (L mol ⁻¹)	R^2	RMS	
298.15	0.08058	1.34×10^5	0.8207	0.312	
308.15	0.08800	2.59×10^5	0.9149	0.254	
318.15	0.10110	1.78×10^5	0.9432	0.277	
328.15	0.09640	2.42×10^5	0.9511	0.236	
Treated					
Langmuir					
T (K)	q_m (mg g ⁻¹)	K_L (L mg ⁻¹)	R^2	RMS	
298.15	168.83	6.15×10^{-2}	0.8546	0.132	
308.15	239.61	4.17×10^{-2}	0.8455	0.074	
318.15	264.50	5.73×10^{-2}	0.5084	0.140	
328.15	189.94	1.59×10^{-1}	0.7343	0.174	
Freundlich					
T (K)	n_F	K_F [mg g ⁻¹ (L mg ⁻¹) ^{1/n}]	R^2	RMS	
298.15	2.17	19.49	0.9584	0.073	
308.15	1.27	10.49	0.9257	0.102	
318.15	1.76	22.78	0.9207	0.115	
328.15	2.53	38.74	0.9344	0.090	
D-R					
T (K)	q_s (mol kg ⁻¹)	K_{DR} (kJ ² mol ⁻²)	R^2	RMS	E (kJ mol ⁻¹)
298.15	1.504	3.16×10^{-3}	0.9278	0.099	7.95×10^{-2}
308.15	11.491	5.66×10^{-3}	0.9469	0.085	1.06×10^{-1}
318.15	3.172	3.30×10^{-3}	0.8915	0.139	8.12×10^{-2}
328.15	1.469	2.00×10^{-3}	0.9044	0.112	6.32×10^{-2}
Temkin					
T (K)	b_T (mol kg ⁻¹)	K_T (L mol ⁻¹)	R^2	RMS	
298.15	0.0655	1.06×10^6	0.7580	0.400	
308.15	0.1306	2.42×10^5	0.9487	0.294	
318.15	0.0901	1.02×10^6	0.6919	0.523	
328.15	0.0623	6.61×10^6	0.6721	0.439	

Table 3 Adsorption capacities of the different biosorbents for the methylene blue model molecule

Adsorbent material	pH	T (K)	q_{max} (mg g ⁻¹)	References
Seed pods from <i>Capparis flexuosa</i>	10.0	298	280.78	Yamil et al. (2020)
<i>Araticum</i> seed powder	7.5	328	300.90	Franco et al. (2020)
Pará chestnut husks	6.5	298	83.8	Georgin et al. (2018)
Dragon fruit peels	5.6	303	192.31	Jawad et al. (2018)
Sugarcane bagasse	10.0	298	17.43	Meili et al. (2019)
Soursop residue	10.0	298	55.30	Meili et al. (2019)
Functionalized peanut husks	8.0	313	43.5	Aryee et al. (2020)
Brazilian berry seeds	8.0	328	189.60	Georgin et al. (2020)
Untreated atemoya peels	7.0	318	190.18	This work
Treated atemoya peels	7.0	318	264.50	This work

Fig. 7 Isothermal equilibria of the removal of methylene blue at different temperatures for the (a) untreated and (b) alkaline-treated atemoya biosorbent. The mixtures were stirred for 12 h at 150 rpm, with an initial pH of 7.00 and different initial concentrations (10, 25, 50, 75, 100, 150, and 200 mg L⁻¹)

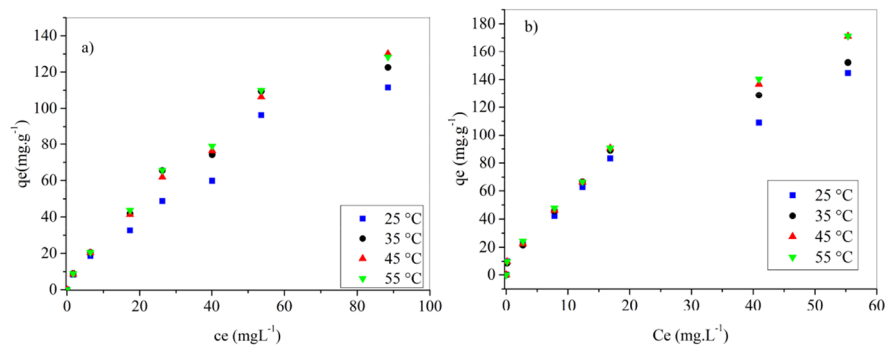
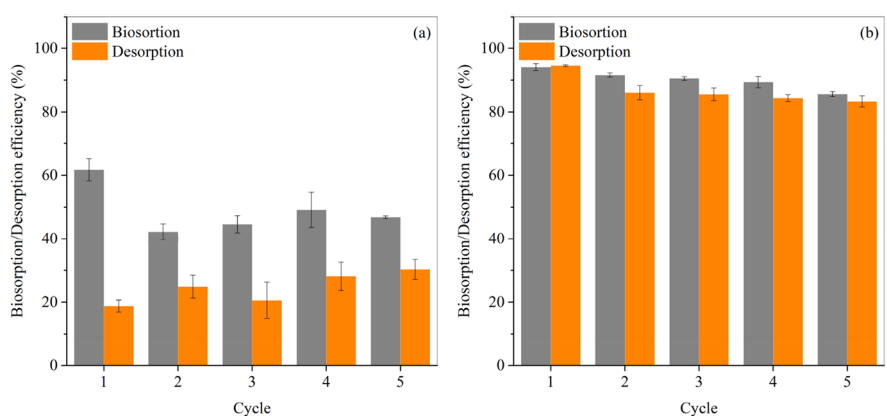


Fig. 8 Efficiency of biosorption/desorption for the (a) untreated and (b) treated atemoya biosorbents. Methylene blue concentration = 50 mg L⁻¹, initial pH = 7.00, stirred for 1 h at 150 rpm



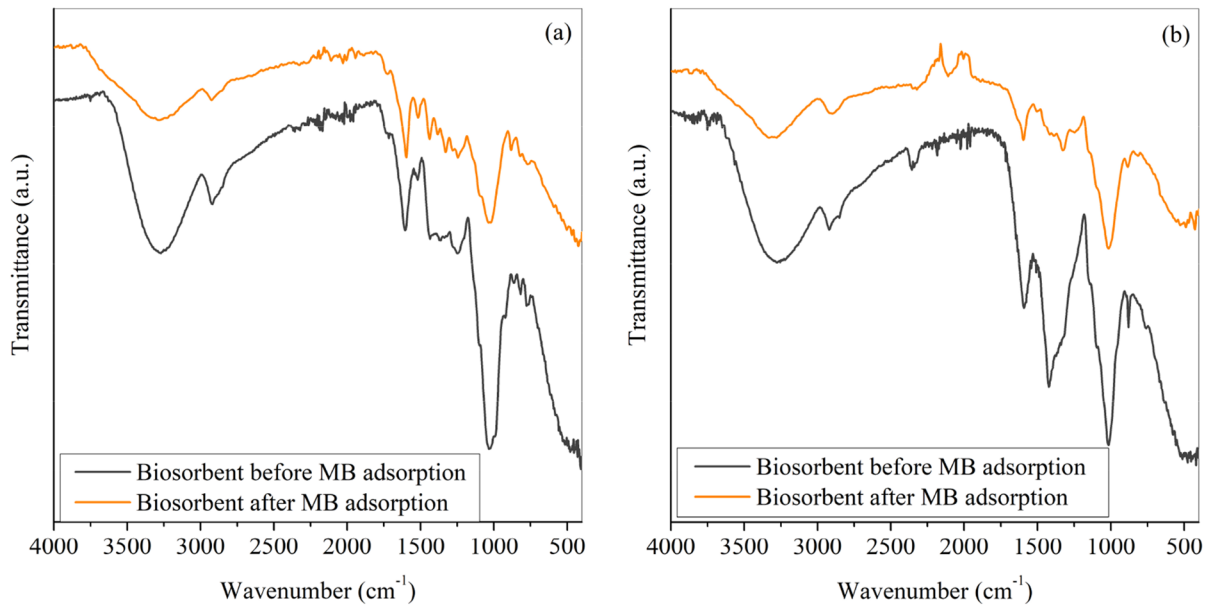


Fig. 9 Infrared spectra of the (a) untreated and (b) alkaline-treated atemoya biosorbents after adsorption of methylene blue (50 mg L^{-1} , initial $\text{pH}=7.00$, 12 h constant stirring at

150 rpm , and room temperature ($25 \pm 2 \text{ }^\circ\text{C}$), then filtered and dried in oven at $40 \pm 2 \text{ }^\circ\text{C}$ for 24 h)

Table 4 Main band shifts observed in the infrared spectra after methylene blue adsorption

Untreated		Alkaline-treated	
Wavelength (cm^{-1})		Wavelength (cm^{-1})	
Before	After	Before	After
1605	1593	1598	1588
1423/1364	Separation and decrease	1419	1330

and untreated biosorbents. These results provide evidence that the adsorption of methylene blue occurred in materials with and without alkaline treatment. Xia et al. (2015), working with magnetically modified yeasts and methylene blue adsorption, obtained a similar profile.

4 Conclusions

The biosorbents prepared from the atemoya peel agricultural waste were characterized using infrared spectra, thermogravimetry, and scanning electronic microscopy, demonstrating that the alkaline-treated

biosorbent was more efficient in removing the methylene blue model molecule. Positive changes in the morphology, porosity, thermal stability, and adsorption efficiency of the material were observed. Experimental adsorption data were adjusted using the D-R model and pseudo-second-order kinetics over a wide pH range, indicating that the adsorption mechanism is chemisorption. Moreover, the alkaline-treated biosorbent proved to be reusable for at least 5 cycles, with a removal efficiency in the range of 80%, indicating that it is a good low-cost alternative for removing cationic effluents and that it could potentially substitute other more expensive adsorbents. Thus, it could be able to minimize the environmental impacts caused by the indiscriminate discharge of effluents into aquatic systems, while reducing the costs of treatment of wastes destined to be either discharged or reused in production processes.

Acknowledgements The authors would like to thank the Laboratory of Electronic Microscopy and Ultrastructural Analysis of the Federal University of Lavras and Finep, Fapemig, CNPq, and Capes for supplying the equipment and technical support for the experiments involving electron microscopy, as well as the Chemical Analysis and Prospection Center (CAPQ/UFLA).

Author Contribution Adneia de Fátima Abreu Venceslau: conceptualization, methodology, validation, investigation, writing—original draft, writing—review and editing.

Andressa Campos Mendonça: methodology, validation, investigation, formal analysis, writing—review and editing.

Lucas Bragança Carvalho: conceptualization, validation, formal analysis, writing—review and editing.

Guilherme Max Dias Ferreira: formal analysis, writing—review and editing.

Sergio Scherrer Thomasi: conceptualization, resources.

Luciana Matos Alves Pinto: conceptualization, resources, writing—review and editing, supervision.

Funding This study was supported in part by the Coordination for the Improvement of Higher Education Personnel—Brazil (CAPES)—Finance Code 001 and Institutional Scientific Initiation Scholarship Program – PIBIC/UFLA.

Data availability All data generated or analyzed during this study are included in this published article (and its supplementary information files).

Declarations

Ethics Approval and Consent to Participate Not applicable.

Consent for Publication Not applicable.

Competing Interests The authors declare no competing interests.

References

- Araújo, C. S. T., Almeida, I. L. S., Rezende, H. C., Marcionilio, S. M. L. O., Léon, J. J. L., & de Matos, T. N. (2018). Elucidation of mechanism involved in adsorption of Pb (II) onto lobeira fruit (*Solanum lycocarpum*) using Langmuir, Freundlich and Temkin isotherms. *Microchemical Journal*, *137*, 348–354.
- Aryee, A. A., Mpatani, F. M., Kani, A. N., Dovi, E., Han, R., Li, Z., & Qu, L. (2020). Iminodiacetic acid functionalized magnetic peanut husk for the removal of methylene blue from solution: Characterization and equilibrium studies. *Environmental Science and Pollution Research*, 1–15
- Bafana, A., Devi, S. S., & Chakrabarti, T. (2011). Azo dyes: Past, present and the future. *Environmental Reviews*, *19*(NA), 350–371.
- Balarak, D., Mostafapour, F. K., Azarpira, H., & Joghataei, A. (2017). Langmuir, Freundlich, Temkin and Dubinin–radushkevich isotherms studies of equilibrium sorption of ampicilin unto montmorillonite nanoparticles. *Journal of Pharmaceutical Research International*, 1–9
- Baron, D., Amaro, A. C. E., Macedo, A. C., Boaro, C. S. F., & Ferreira, G. (2018). Physiological changes modulated by rootstocks in atemoya (*Annona x atemoya* Mabb.): Gas exchange, growth and ion concentration. *Brazilian Journal of Botany*, *41*(1), 219–225.
- Biehl, P., von der Lühne, M., & Schacher, F. H. (2018). Reversible adsorption of methylene blue as cationic model cargo onto polyzwitterionic magnetic nanoparticles. *Macromolecular Rapid Communications*, *39*(14), 1800017.
- Carneiro, P. A., Umbuzeiro, G. A., Oliveira, D. P., & Zanoni, M. V. B. (2010). Assessment of water contamination caused by a mutagenic textile effluent/dyehouse effluent bearing disperse dyes. *Journal of Hazardous Materials*, *174*(1–3), 694–699.
- Carvalho, L. B., Chagas, P. M. B., Marques, T. R., Razafitianamaharavo, A., Pelletier, M., Nolis, P., ... Pinto, L. d. M. A. (2019). Removal of the synthetic hormone methyltestosterone from aqueous solution using a β -cyclodextrin/silica composite. *Journal of Environmental Chemical Engineering*, *7*(6), 103492. <https://doi.org/10.1016/j.jece.2019.103492>
- Carvalho, L. B., Chagas, P. M. B., & Pinto, L. M. A. (2018). *Caesalpinia ferrea* fruits as a biosorbent for the removal of methylene blue dye from an aqueous medium. *Water, Air, & Soil Pollution*, *229*(9), 297.
- Chen, S. G., & Yang, R. T. (1994). Theoretical basis for the potential theory adsorption isotherms The Dubinin–Radushkevich and Dubinin–Astakhov Equations. *Langmuir*, *10*(11), 4244–4249.
- Chieng, H. I., Lim, L. B. L., & Priyantha, N. (2017). Enhancement of crystal violet dye adsorption on *Artocarpus camansi* peel through sodium hydroxide treatment. *Desalination and Water Treatment*, *58*, 320–331.
- Cooksey, C. J. (2017). Quirks of dye nomenclature. 8. Methylene blue, azure and violet. *Biotechnique & Histochemistry*, *92*(5), 347–356.
- Costa, E. V., Pinheiro, M. L. B., Xavier, C. M., Silva, J. R. A., Amaral, A. C. F., Souza, A. D. L., ... Machado, G. M. C. (2006). A pyrimidine- β -carboline and other alkaloids from *Annona foetida* with antileishmanial activity. *Journal of natural products*, *69*(2), 292–294
- Cruz, L. S. D., Lima, R. Z., Abreu, C. M. P. D., Corrêa, A. D., & Pinto, L. D. M. A. (2013). Physical and chemical characterization of fractions of fruit atemoya *Gefner*. *Ciência Rural*, *43*(12), 2280–2284.
- Dada, A. O., Olalekan, A. P., Olatunya, A. M., & Dada, O. (2012). Langmuir, Freundlich, Temkin and Dubinin–Radushkevich isotherms studies of equilibrium sorption of Zn²⁺ unto phosphoric acid modified rice husk. *IOSR Journal of Applied Chemistry*, *3*(1), 38–45.
- de Souza, P. A., da Silva Freitas, R. V., Batista, E. M., da Costa, F. B., & Maracajá, P. B. (2015). Armazenamento de atemoias, *Annona squamosa* x *Annona cherimola*, recobertas com filme PVC. *Revista Verde De Agroecologia e Desenvolvimento Sustentável*, *10*(5), 39.
- Dutta, M., Islam, N., Rabha, S., Narzary, B., Bordoloi, M., Saikia, D., ... Saikia, B. K. (2020). Acid mine drainage in an Indian high-sulfur coal mining area: Cytotoxicity assay

- and remediation study. *Journal of Hazardous Materials*, 389, 121851. <https://doi.org/10.1016/j.jhazmat.2019.121851>
- El-Naggar, N.E.-A., & Rabei, N. H. (2020). Bioprocessing optimization for efficient simultaneous removal of methylene blue and nickel by *Gracilaria* seaweed biomass. *Scientific Reports*, 10(1), 1–21.
- Enniya, I., & Jourani, A. (2017). Study of Methylene Blue Removal by a biosorbent prepared with Apple peels. *J. Mater. Environ. Sci.*, 8(12), 4573–4581.
- Ferrari, V., Taffarel, S. R., Espinosa-Fuentes, E., Oliveira, M. L. S., Saikia, B. K., & Oliveira, L. F. S. (2019). Chemical evaluation of by-products of the grape industry as potential agricultural fertilizers. *Journal of Cleaner Production*, 208, 297–306.
- Fomina, M., & Gadd, G. M. (2014). Biosorption: Current perspectives on concept, definition and application. *Bioresour. Technol.*, 160, 3–14.
- Foo, K. Y., & Hameed, B. H. (2009). An overview of landfill leachate treatment via activated carbon adsorption process. *Journal of Hazardous Materials*, 171(1–3), 54–60.
- Franco, D. S. P., Georgin, J., Drumm, F. C., Netto, M. S., Allasia, D., Oliveira, M. L. S., & Dotto, G. L. (2020). Araticum (*Annona crassiflora*) seed powder (ASP) for the treatment of colored effluents by biosorption. *Environmental Science and Pollution Research*, 27(10), 11184–11194.
- Freundlich, H. (1907). Über die adsorption in lösungen. *Zeitschrift Für Physikalische Chemie*, 57(1), 385–470.
- Georgin, J., Franco, D. S. P., Netto, M. S., Allasia, D., Oliveira, M. L. S., & Dotto, G. L. (2020). Treatment of water containing methylene by biosorption using Brazilian berry seeds (*Eugenia uniflora*). *Environmental Science and Pollution Research*, 1–13.
- Georgin, J., Marques, B. S., Peres, E. C., Allasia, D., & Dotto, G. L. (2018). Biosorption of cationic dyes by *Pará* chestnut husk (*Bertholletia excelsa*). *Water Science and Technology*, 77(6), 1612–1621.
- Gerola, G. P., Boas, N. V., Caetano, J., Tarley, C. R. T., Gonçalves, A. C., & Dragunski, D. C. (2013). Utilization of passion fruit skin by-product as lead (II) ion biosorbent. *Water, Air, & Soil Pollution*, 224(2), 1446.
- Ho, Y.-S., & McKay, G. (1999). Pseudo-second order model for sorption processes. *Process Biochemistry*, 34(5), 451–465.
- Jawad, A. H., Kadhum, A. M., & Ngoh, Y. S. (2018). Applicability of dragon fruit (*Hylocereus polyrhizus*) peels as low-cost biosorbent for adsorption of methylene blue from aqueous solution: Kinetics, equilibrium and thermodynamics studies. *Desalination and Water Treatment*, 109, 231–240.
- Juchen, P. T., Piffer, H. H., Veit, M. T., da Cunha Gonçalves, G., Palácio, S. M., & Zanette, J. C. (2018). Biosorption of reactive blue BF-5G dye by malt bagasse: Kinetic and equilibrium studies. *Journal of Environmental Chemical Engineering*, 6(6), 7111–7118. <https://doi.org/10.1016/j.jece.2018.11.009>
- Kariuki, Z., Kiptoo, J., & Onyancha, D. (2017). Biosorption studies of lead and copper using rogers mushroom biomass ‘*Lepiota hystrix*.’ *South African Journal of Chemical Engineering*, 23, 62–70.
- Khadir, A., Negarestani, M., & Ghiasinejad, H. (2020). Low-cost sisal fibers/polypyrrole/polyaniline biosorbent for sequestration of reactive orange 5 from aqueous solutions. *Journal of Environmental Chemical Engineering*, 8(4), 103956. <https://doi.org/10.1016/j.jece.2020.103956>
- Kilic, M., Apaydin-Varol, E., & Pütün, A. E. (2011). Adsorptive removal of phenol from aqueous solutions on activated carbon prepared from tobacco residues: Equilibrium, kinetics and thermodynamics. *Journal of Hazardous Materials*, 189(1–2), 397–403.
- Kumara, P. S., Joshibaa, G. J., Feminaa, C. C., Varshinia, P., Priyadharshinia, S., Karthicka, M. A., & Jothirani, R. (2019). A critical review on recent developments in the low-cost adsorption of dyes from wastewater. *Desalination and Water Treatment*, 172, 395–416.
- Kwak, J.-H., Islam, M. S., Wang, S., Messele, S. A., Naeth, M. A., El-Din, M. G., & Chang, S. X. (2019). Biochar properties and lead (II) adsorption capacity depend on feedstock type, pyrolysis temperature, and steam activation. *Chemosphere*, 231, 393–404.
- Lagergren, S. K. (1898). About the theory of so-called adsorption of soluble substances. *Sven Vetenskapsakad Handlingar*, 24, 1–39.
- Langmuir, I. (1916). The constitution and fundamental properties of solids and liquids Part I. Solids. *Journal of the American chemical society*, 38(11), 2221–2295.
- Lin, S.-H., & Juang, R.-S. (2002). Heavy metal removal from water by sorption using surfactant-modified montmorillonite. *Journal of Hazardous Materials*, 92(3), 315–326.
- Mateo-Sagasta, J., Zadeh, S. M., Turrall, H., & Burke, J. (2017). *Water pollution from agriculture: A global review. Executive summary*. Rome, Italy: FAO Colombo, Sri Lanka: International Water Management ...
- Meili, L., Lins, P. V. S., Costa, M. T., Almeida, R. L., Abud, A. K. S., Soletti, J. I., ... Carvalho, S. H. V. (2019). Adsorption of methylene blue on agroindustrial wastes: Experimental investigation and phenomenological modelling. *Progress in biophysics and molecular biology*, 141, 60–71
- Mohamed, M. A., Salleh, W. N. W., Jaafar, J., Ismail, A. F., Abd Mutalib, M., Mohamad, A. B., ... Hir, Z. A. M. (2017). Physicochemical characterization of cellulose nanocrystal and nanoporous self-assembled CNC membrane derived from *Ceiba pentandra*. *Carbohydrate Polymers*, 157, 1892–1902
- Mohtar, S. S., Busu, T. N. Z. T. M., Noor, A. M. M., Shaari, N., Yusoff, N. A., Bustam, M. A., ... Mat, H. B. (2015). Extraction and characterization of lignin from oil palm biomass via ionic liquid dissolution and non-toxic aluminium potassium sulfate dodecahydrate precipitation processes. *Bioresour. Technol.*, 192, 212–218
- Mokhtar, N., Aziz, E. A., Aris, A., Ishak, W. F. W., & Mohd Ali, N. S. (2017). Biosorption of azo-dye using marine macro-alga of *Euchema spinosum*. *Journal of Environmental Chemical Engineering*, 5(6), 5721–5731. <https://doi.org/10.1016/j.jece.2017.10.043>
- Morton, J. F. (1987). *Fruits of warm climates*. JF Morton.

- Novais, R. M., Ascensao, G., Tobaldi, D. M., Seabra, M. P., & Labrincha, J. A. (2018). Biomass fly ash geopolymer monoliths for effective methylene blue removal from wastewaters. *Journal of Cleaner Production*, 171, 783–794.
- Pérez-Morales, J. M., Sánchez-Galván, G., & Olgún, E. J. (2019). Continuous dye adsorption and desorption on an invasive macrophyte (*Salvinia minima*). *Environmental Science and Pollution Research*, 26(6), 5955–5970.
- Rafatullah, M., Sulaiman, O., Hashim, R., & Ahmad, A. (2010). Adsorption of methylene blue on low-cost adsorbents: A review. *Journal of Hazardous Materials*, 177(1–3), 70–80.
- Ramrakhiani, L., Ghosh, S., & Majumdar, S. (2016). Surface modification of naturally available biomass for enhancement of heavy metal removal efficiency, upscaling prospects, and management aspects of spent biosorbents: A review. *Applied Biochemistry and Biotechnology*, 180(1), 41–78.
- Rangabhashiyam, S., Lata, S., & Balasubramanian, P. (2018). Biosorption characteristics of methylene blue and malachite green from simulated wastewater onto *Carica papaya* wood biosorbent. *Surfaces and Interfaces*, 10, 197–215.
- Regalbuto, J. R., & Robles, J. (2004). The engineering of Pt/carbon catalyst preparation. *University of Illinois, Chicago*, 1, 1–14.
- Richardson, S. D., & Ternes, T. A. (2018). Water analysis: Emerging contaminants and current issues. *Analytical Chemistry*, 90(1), 398–428. <https://doi.org/10.1021/acs.analchem.7b04577>
- Rojo, E., Alonso, M. V., Domínguez, J. C., Saz-Orozco, B. D., Oliet, M., & Rodríguez, F. (2013). Alkali treatment of viscose cellulosic fibers from eucalyptus wood: structural, morphological, and thermal analysis. *Journal of Applied Polymer Science*, 130(3), 2198–2204.
- Rudzinski, W., & Plazinski, W. (2007). Studies of the kinetics of solute adsorption at solid/solution interfaces: On the possibility of distinguishing between the diffusional and the surface reaction kinetic models by studying the pseudo-first-order kinetics. *The Journal of Physical Chemistry C*, 111(41), 15100–15110.
- Sadaf, S., & Bhatti, H. N. (2014). Batch and fixed bed column studies for the removal of Indosol Yellow BG dye by peanut husk. *Journal of the Taiwan Institute of Chemical Engineers*, 45(2), 541–553.
- Schwanninger, M., Rodrigues, J. C., & Fackler, K. (2011). A review of band assignments in near infrared spectra of wood and wood components. *Journal of near Infrared Spectroscopy*, 19(5), 287–308.
- Sellaoui, L., Hessou, E. P., Badawi, M., Netto, M. S., Dotto, G. L., Silva, L. F. O., ... Chen, Z. (2021a). Trapping of Ag⁺, Cu²⁺, and Co²⁺ by faujasite zeolite Y: New interpretations of the adsorption mechanism via DFT and statistical modeling investigation. *Chemical Engineering Journal*, 420, 127712.
- Sellaoui, L., Yazidi, A., Ali, J., Dotto, G. L., Bonilla-Petriciolet, A., Oliveira, L. F. S., & Chen, Z. (2021b). Theoretical study and analysis of o-nitrophenol adsorption using layered double hydroxides containing Ca-Al, Ni-Al and Zn-Al. *Environmental Science and Pollution Research*, 28(32), 44547–44556. <https://doi.org/10.1007/s11356-021-13882-x>
- Shanmugarajah, B., Chew, I. M., Mubarak, N. M., Choong, T. S., Yoo, C., & Tan, K. (2019). Valorization of palm oil agro-waste into cellulose biosorbents for highly effective textile effluent remediation. *Journal of Cleaner Production*, 210, 697–709.
- Sharma, S., Hasan, A., Kumar, N., & Pandey, L. M. (2018). Removal of methylene blue dye from aqueous solution using immobilized *Agrobacterium fabrum* biomass along with iron oxide nanoparticles as biosorbent. *Environmental Science and Pollution Research*, 25(22), 21605–21615.
- Silva, G. M. C., da Silva, M. P. S., Biazatti, M. A., dos Santos, P. C., da Silva, N. M., & Mizobutsi, G. P. (2016). Uso do 1-MCP e atmosfera modificada na pós-colheita de atemoia ‘Gefner.’ *Revista Brasileira De Ciências Agrárias*, 11(2), 67–72.
- Silva, N. F., Netto, M. S., Silva, L. F. O., Mallmann, E. S., Lima, E. C., Ferrari, V., & Dotto, G. L. (2021). Composite carbon materials from winery composted waste for the treatment of effluents contaminated with ketoprofen and 2-nitrophenol. *Journal of Environmental Chemical Engineering*, 9(4), 105421. <https://doi.org/10.1016/j.jece.2021.105421>
- Singh, R. L., Singh, P. K., & Singh, R. P. (2015). Enzymatic decolorization and degradation of azo dyes—A review. *International Biodeterioration & Biodegradation*, 104, 21–31.
- Sivakumar, R., Renganathan, P. S., Helan, H. M., & Rajachandrasekar, T. (2019). Removal of copper ion from aqueous solution using seeds of sugar apple (*Annona squamosa* L.).
- Smoczyński, L., Pierożyński, B., & Mikołajczyk, T. (2020). The effect of temperature on the biosorption of dyes from aqueous solutions. *Processes*, 8(6), 636.
- Temkin, M., & Pyzhev, V. (1940). Kinetics of the synthesis of ammonia on promoted iron catalysts. *Jour Phys Chem (USSR)*, 13, 851–867.
- Tkaczyk, A., Mitrowska, K., & Posyniak, A. (2020). Synthetic organic dyes as contaminants of the aquatic environment and their implications for ecosystems: A review. *Science of The Total Environment*, 717, 137222
- Tran, H. N., You, S.-J., Hosseini-Bandegharai, A., & Chao, H.-P. (2017). Mistakes and inconsistencies regarding adsorption of contaminants from aqueous solutions: A critical review. *Water Research*, 120, 88–116.
- Tsai, W.-T., Hsu, C.-H., & Lin, Y.-Q. (2019). Highly porous and nutrients-rich biochar derived from dairy cattle manure and its potential for removal of cationic compound from water. *Agriculture*, 9(6), 114.
- Vithanage, M., Mayakaduwa, S. S., Herath, I., Ok, Y. S., & Mohan, D. (2016). Kinetics, thermodynamics and mechanistic studies of carbofuran removal using biochars from tea waste and rice husks. *Chemosphere*, 150, 781–789.
- Venceslau, A.F.A.; Mendonça, A.C.; Benedick, L.A.Z.; Thomasi, S.S.; Nunes, C.A.; Pinto, L.M.A. (2021). Analysis of the chemical constituents of *Thompson* atemoia seed oil. *Revista Brasileira de Fruticultura*, 43(6)
- Weber, W. J., & Morris, J. C. (1963). Kinetics of adsorption on carbon from solution. *Journal of the Sanitary Engineering Division*, 89(2), 31–60.
- Xia, S., Zhang, L., Pan, G., Qian, P., & Ni, Z. (2015). Photocatalytic degradation of methylene blue with a nanocomposite

- system: synthesis, photocatalysis and degradation pathways. *Physical Chemistry Chemical Physics*, 17(7), 5345–5351.
- Yanishpolskii, V. V., Skubiszewska-Zieba, J., Leboda, R., Tertykh, V. A., & Klischar, I. V. (2000). Methylene Blue Sorption Equilibria on Hydroxylated Silica Surfaces as Well as on Carbon–Silica Adsorbents (Carbosils). *Adsorption Science & Technology*, 18(2), 83–95.
- Yamil, L. d. O., Georjgin, J., Franco, D. S. P., Netto, M. S., Foletto, E. L., Piccilli, D. G. A., ... Dotto, G. L. (2020). Transforming pods of the species *Capparis flexuosa* into effective biosorbent to remove blue methylene and bright blue in discontinuous and continuous systems. *Environmental Science and Pollution Research*, 1–14.

Publisher's Note Springer Nature remains neutral with regard to jurisdictional claims in published maps and institutional affiliations.